Int J Adv Manuf Technol (2017) 92:1465–1480
DOI 10.1007/s00170-017-0229-x

ORIGINAL ARTICLE

Identification and modeling of cutting forces in ball-end milling based on two different finite element models with Arbitrary Lagrangian Eulerian technique

Mehmet Aydın [1] · **Uğur Köklü** [2]

Received: 7 November 2016 / Accepted: 26 February 2017 / Published online: 13 March 2017

Abstract This paper presents two different finite element (FE) models with Arbitrary Lagrangian Eulerian (ALE) technique to evaluate the effectiveness of FE modeling for estimating the cutting forces in ball-end milling. The milling forces are modeled using a unified mechanics of the cutting approach, which is based on the shear stress, friction coefficient and chip thickness ratio provided through the orthogonal cutting process. Two-dimensional (2D) FE models of the orthogonal cutting are designed for estimating the milling forces using this approach, and explicit dynamic thermo-mechanical analyses are performed to determine the orthogonal cutting data from a set of cutting and material parameters. The oblique transformation approach is used to carry the orthogonal cutting data to the milling cutter geometry. Simulations are numerically and analytically carried out for machining of 20NiCrMo5 material with a tungsten carbide tool and the estimated forces are compared to measured ones. The estimation of milling forces is accurately achieved by the unified mechanics of cutting approach with orthogonal cutting data based on the ALE technique using Eulerian-Lagrangian boundaries. Good agreements between the estimated and measured outcomes reveal an obvious knowledge of an efficient and accurate FE model for determining the ball-end milling forces.

✉ Mehmet Aydın
mehmet.aydin@bilecik.edu.tr

[1] Department of Industrial Product Design, Bilecik Şeyh Edebali University, 11230 Bilecik, Turkey

[2] Department of Mechanical Engineering, Karamanoğlu Mehmetbey University, 70100 Karaman, Turkey

Keywords ALE technique · Ball-end milling · Cutting forces · FE modeling · Orthogonal cutting

1 Introduction

The accuracy of numerical estimation of the machining variables such as shear stress, friction angle and chip thickness ratio is of vital importance for analytically estimating the cutting forces in ball-end milling processes. Workpiece flow stress, thermal and mechanical properties, friction and heat transfer parameters, material fracture criterion and modeling approach highly influence the validity of the outcomes estimated from the cutting process based on the finite element (FE) method. Therefore, there is uncertainty about the effectiveness of FE-based cutting simulations. It is necessary to build more efficient FE models for estimating the accurate process variables.

Estimations of cutting forces are considered to calculate tool deflection and wear, workpiece deflection and surface errors in addition to identifying the strengths of jigs and fixtures and the power requirements. The mechanistic model is frequently utilized for estimating the cutting force [1–4], surface error [5] and tool wear [6], where the cutting force coefficients are approximated by curve fit to experimental cutting forces. Uriarte et al. [7] extended the mechanistic model to estimate the cutting forces in micro-scale machining of AISI H13 tool steel with two-fluted carbide milling cutters. The mechanistic model requires a great deal of experiments and is implementable for a particular tool–workpiece combination. It is not so practical in ball-end milling because of the use of milling cutters with complex geometry. To avoid such limitations, Budak et al. [8] offered a unified mechanics of cutting approach for estimating the cutting forces, which was based on a cutting database extracted from orthogonal cutting

experiments. Wan et al. [9] developed a unified force model to determinate the shear stress and friction angle etc. by transforming the experimental milling forces into a local coordinate system. Lee and Altıntaş [10] improved the unified mechanics approach for ball-end milling. They used the classical oblique cutting method to carry the orthogonal cutting data to ball-end milling edge geometry. Wei et al. [11] suggested a method considering the shearing and plowing mechanisms for estimating the cutting forces in ball-end milling of sculptured surfaces. Cao et al. [12] studied some aspects of the cutter eccentricity to precisely estimate the cutting forces in ball-end milling.

FE modeling-based techniques have been commonly utilized to study cutting forces in conventional milling processes [13]. As it is known, there are two main formulations in FE simulations of deformation processes: Eulerian and Lagrangian. The FE mesh deforms with the material in Lagrangian formulation. In Eulerian formulation, the mesh is stationary spatially, and thus mesh distortion does not occur. In those analyses, implicit and explicit integration approaches are utilized for time discretization. The implicit approach is applied to solve linear static problems whereas the explicit approach is appropriate for nonlinear dynamic situations. Prasad [14] introduced a FE model to consider the residual stress on the workpiece in the orthogonal cutting of the 20NiCrMo5 steel. This model was based on the explicit integration approach with Lagrangian boundary condition. Miguélez et al. [15] presented a plane-strain model to analyze shear banding in machining of Ti6Al4V material using 2D FE code with Lagrangian formulation. Duan and Zhang [16] constructed an orthogonal cutting model to accurately simulate a high-speed cutting process. The model was based on the implicit Lagrangian formulation which has a stable remeshing property. Other researches using the Lagrangian approach were performed by Ye et al. [17], Ducobu et al. [18] and Zhang et al. [19]. However, the Lagrangian approach requires a chip separation criterion. Thus, a variety of criteria such as effective strain criterion and strain energy density are utilized for chip formation simulations. On the other hand, the Eulerian formulation is applied to avoid the use of a failure criterion for chip formation. Strenkowski et al. [20] used the Eulerian FE technique for estimating the force components and chip flow angle when orthogonal cutting AISI 1020 steel. Raczy et al. [21] presented an Eulerian FE model with two different material models, elastic-plastic hydrodynamic and Johnson–Cook (J-C), for modeling orthogonal cutting of purity copper. The Arbitrary Lagrangian Eulerian (ALE) formulation is a relatively new modeling technique used in analyzing nonlinear situations, involving the Lagrangian and Eulerian ones without their disadvantages. During adaptive meshing, a smooth mesh in the ALE domain is reproduced by utilizing appropriate parameter settings and mesh distribution, and analysis parameters such as density, energy and thermo-mechanical variables are adapted from the old mesh to the renewed one. The mesh quality is controlled by continuous meshing and advection as the FE analysis progresses. The ALE models have been utilized in cutting simulations by Arrazola and Özel [22], Adetoro and Wen [23] and Aydin [24].

As can be seen from the above literature, Lagrangian, Eulerian and ALE formulations are commonly employed in FE modeling of machining. The capabilities of FE models should be taken into consideration to obtain the satisfactory results of process variables. The present study analyzes the capabilities of FE modeling approaches having two different ALE techniques which are developed to precisely and realistically estimate ball-end milling forces. For that purpose, explicit dynamic thermo-mechanical analyses are carried out to study the influences of FE modeling involving distinct ALE approaches when simulating cutting of 20NiCrMo5 steel with continuous chip formation. Relying upon the study of Lee and Altıntaş [10], the milling forces are analytically modeled from the orthogonal cutting data. The capabilities of the numerical approaches are demonstrated by the comparison of the estimated and measured force components. The simulation results indicate that the predictive approach, namely unified mechanics of cutting approach, together with orthogonal cutting data identified numerically from the ALE technique with Eulerian–Lagrangian boundaries, can more precisely estimate milling force components for a ball-end milling cutter.

2 FE modeling of cutting process

In this study, two different plane-strain ALE FE models with the FE code ABAQUS/Explicit have been developed for the identification of the milling forces from orthogonal cutting simulations and the unified mechanics of cutting approach. Firstly, an ALE FE model with Lagrangian boundaries was established. In this approach, the mesh was connected to the material and it followed the material throughout the simulation. This technique needs no initial chip geometry for metal cutting simulation. However, high mesh distortions are a matter of concern for Lagrangian formulation. Besides, a chip separation criterion has to be defined. Secondly, an ALE FE model with Eulerian–Lagrangian boundaries was designed. This technique reduces the typical element distortion problem of the Lagrangian approach, but requires an initial chip shape. A criterion was not used for chip separation in this FE model.

The cutting process causes large deformations, resulting in mesh distortion and termination of the FE analysis. Therefore, it is tremendously significant to employ adaptive meshing with fine-tuned parameters. In this study, the frequency was taken as 1 for remeshing. During each adaptive meshing increment, the new mesh was constructed by performing five remeshing sweeps and then the solution variables were

mapped to the new mesh to reduce element distortion. For the mesh-update procedure, uniform mesh smoothing was used and the new mesh was estimated from the current node positions. The curvature refinement was taken as 2 to drag nodes to areas where the mesh density was decreased. A volume-weighted average algorithm was utilized for the relocation of the nodes when large mesh distortions occurred. Because of its computational efficiency, an element center projection algorithm with a second order was chosen for the stress update.

The explicit dynamic thermo-mechanical FE models were developed by including thermal and mechanical properties presented in Table 1. The tungsten carbide tool was modeled as a rigid body while the workpiece was defined as a deformable body. Table 2 summarizes the cutting parameters and tool geometry. For all cutting conditions, the chip was supposed as continuous. The workpiece material was 20NiCrMo5 steel. The material behavior of the workpiece was described by the J-C model [25] as proposed by Stenberg and Proudian [26].

$$\overline{\sigma} = \left[490 + 600\left(\varepsilon^{pl}\right)^{0.21}\right]\left[1 + 0.015\ \mathrm{In}\left(\frac{\dot{\varepsilon}^{pl}}{\dot{\varepsilon}_0}\right)\right]\left[1-\left(\frac{T-20}{1900-20}\right)^{0.6}\right] \quad (1)$$

Where, $\overline{\sigma}$ is the flow stress (MPa), ε^{pl} is the plastic strain, $\dot{\varepsilon}^{pl}$ is the plastic strain rate, $\dot{\varepsilon}_0$ is the reference strain rate ($1.0/s^1$) and T is the temperature of the workpiece material (°C).

The workpiece and tool models were meshed using the quadrilateral elements with reduced integration and hourglass control. To model large deformations expected in the chip, three different mesh sizes were considered in the ALE FE models, namely meshx1, meshx2 and meshx3. Table 3 shows the values of the mesh sizes. The tool was also composed of 1195 four-node plane-strain elements with 1266 nodes.

2.1 ALE FE model with Lagrangian boundaries

A schematic representation of the ALE FE model using Lagrangian boundaries for the orthogonal cutting simulations is given in Fig. 1. The bottom edge of the workpiece was fully restrained against any displacement. The tool was constrained both rotationally and translationally in the y direction at the reference node while a translational motion was given in the negative x direction. A parting line was defined for chip separation.

The adaptive mesh domain with Lagrangian boundaries was defined by selecting the whole workpiece. Due to Lagrangian formulation, a chip formation criterion was also introduced to perform realistic simulations. The used numerical approach was a combination of the progressive shear and ductile damage initiation criterion. According to this approach, the material begins to deform when the shear strain comes to the critical plastic strain value. In this study, the critical plastic strain adopted to govern the damage initiation was taken as 1.5 [14].

The tool/chip contact was described between the chip and the outer surface of the tool. In the normal direction, a penalty-based hard contact was applied to model the contact along the tool/chip interface. In the tangential direction, the Coulomb friction model, with a friction coefficient of 0.4 reported by Prasad [14], was used without a shear stress limitation since the chip was defined as a node-based surface.

2.2 ALE FE model with Eulerian–Lagrangian boundaries

The ALE FE model using Eulerian–Lagrangian boundaries needs the predefined chip geometry. Figure 2 schematically shows the boundary conditions for the workpiece and tool geometries. The workpiece was permitted to move horizontally from the left to the right whereas it was arrested to ensure the stability in the y direction. The cutting tool was constrained on its top and right edges.

The workpiece was designed as a 2D shell having Lagrangian boundaries at its top and bottom edges and Eulerian boundaries at the entry-flow, chip-flow and exit-flow sides. In this model with Eulerian–Lagrangian boundaries, a chip separation criterion was not used since the chip formation was simulated through plastic flow of the workpiece material. The chip flow was restricted at a vertical location since the chip was described with the Eulerian boundary at its upper side and the Lagrangian boundary from other sides.

The normal contact along the tool/chip interface was modeled by defining the penalty-based hard contact. For the

Table 1 The material properties of the workpiece and tool [26, 27]

Property	Workpiece (20NiCrMo5)	Tool (tungsten carbide)
Density (kg/m^3)	7800	14,500
Poisson's ratio	0.3	0.227
Young's modulus (Pa)	2.1×10^{11}	5.4×10^{11}
Thermal conductivity (W/m °C)	47.7	84 (20 °C)
		63 (1000 °C)
Specific heat(J/kg °C)	556	220
Thermal expansion (1/°C)	1.2×10^{-6}	5.8×10^{-6}

Table 2 Tool geometry and cutting parameters used in orthogonal cutting

Tool geometry	Rake angle, α (°)	6
	Clearance angle, γ (°)	6
	Cutting edge radius, r_β (μm)	20
Cutting parameters	Cutting speed, V_c (m/s)	0.25–0.75–1.25–2.25–3.5
	Undeformed chip thickness, t (mm)	0.025–0.05–0.075–0.1–0.125
	Depth of cut, a (mm)	3

tangential direction, a modified version of the Coulomb friction model was applied to define contact pair interaction, where a shear stress limit was used.

$$\left.\begin{array}{lll} \tau_p(x) = \tau_{max} & \text{when} & \mu\sigma_n(x) \geq \tau_{max} \\ \tau_p(x) = \mu\ \sigma_n(x) & \text{when} & \mu\sigma_n(x) < \tau_{max} \end{array}\right\} \quad (2)$$

Where, τ_p and σ_n are shear and normal contact stress, respectively, τ_{max} is the shear stress limit and μ is the friction coefficient. Here, shear stress limit of 210 MPa and friction coefficient of 0.4 were used [14].

3 Cutting force modeling of ball-end milling process

The geometry of the ball-end milling cutter and the cutting forces are illustrated in Fig. 3. The flutes have a helix angle (β_0) at the transition from the hemispherical piece into the cylindrical one. Due to the variation of the local cutter radius towards the spherical tip in the Z direction, the local helix angle changes.

To model the ball-end milling forces using the unified mechanics of cutting approach, an orthogonal cutting database that characterizes the tool–workpiece pair is established using the orthogonal cutting model [8]. In this study, four different steps are followed to calculate the ball-end milling forces using the unified mechanics of cutting approach. In the first step, the hemispherical piece of the helical ball-end milling cutter is partitioned into a series of elementary disks along its axis, whose differential length is $dz_{j,i}$. The cutting actions of the disc segments are considered to be oblique cutting processes with an inclination angle equal to the local helix angle ($\beta_{j,i}(\psi)$) and a normal rake angle at the hemispherical piece of the milling cutter($\alpha_{n,j,i}(\psi)$), where index j,i denotes the ith disc segment of the jth flute. In the second step, the chip thickness for each disc segment is determined. In the third step, the orthogonal cutting database is transformed to oblique cutting edge geometry using the oblique transformation model [8]. In the last step, the total instantaneous cutting force acting on the milling cutter is estimated by numerical integration.

The local cutter radius ($r_{j,i}(\psi)$) and local helix angle ($\beta_{j,i}(\psi)$) at axial depth z are expressed in the following form [10]:

$$r_{j,i}(\psi) = \begin{cases} r_0\sqrt{1-[\psi\ \cot(\beta_0)-1]^2} & 0 \leq z < r_0 \\ r_0 & z \geq r_0 \end{cases} \quad (3)$$

$$\beta_{j,i}(\psi) = \begin{cases} \tan^{-1}\left(\dfrac{r_{j,i}(\psi)}{r_0}\tan(\beta_0)\right) & 0 \leq z < r_0 \\ \beta_0 & z \geq r_0 \end{cases} \quad (4)$$

Where, r_0 is the spherical radius of the milling cutter. ψ represents the lag angle between the tip of the flute ($z=0$) and axial depth z because of the helix angle (β_0).

The elementary tangential force ($dF_{t,j,i}(\phi)$), radial force ($dF_{r,j,i}(\phi)$) and axial force ($dF_{a,j,i}(\phi)$) acting on the milling cutter are formulated by [10]

$$\begin{aligned} dF_{t,j,i}(\phi) &= K_{te}\,dS_{j,i} + K_{tc,j,i}\ t_{n,j,i}(\phi_{j,i},\kappa_{j,i})\ db_{j,i} \\ dF_{r,j,i}(\phi) &= K_{re}\,dS_{j,i} + K_{rc,j,i}\ t_{n,j,i}(\phi_{j,i},\kappa_{j,i})\ db_{j,i} \\ dF_{a,j,i}(\phi) &= K_{ae}\,dS_{j,i} + K_{ac,j,i}\ t_{n,j,i}(\phi_{j,i},\kappa_{j,i})\ db_{j,i} \end{aligned} \quad (5)$$

Table 3 Number of elements in the workpiece and element size in the chip for the ALE FE models

Model	Mesh size	Number of elements in the workpiece (t = 0.1 mm)	Element size in the chip (mm)	
			Minimum	Maximum
ALE FE model with Lagrangian boundaries	meshx1	6218	5×10^{-3}	1×10^{-2}
	meshx2	8318	2.5×10^{-3}	5×10^{-3}
	meshx3	12,368	1.25×10^{-3}	2.5×10^{-3}
ALE FE model with Eulerian–Lagrangian boundaries	meshx1	1619	5×10^{-3}	1×10^{-2}
	meshx2	2457	2.5×10^{-3}	5×10^{-3}
	meshx3	4435	1.25×10^{-3}	2.5×10^{-3}

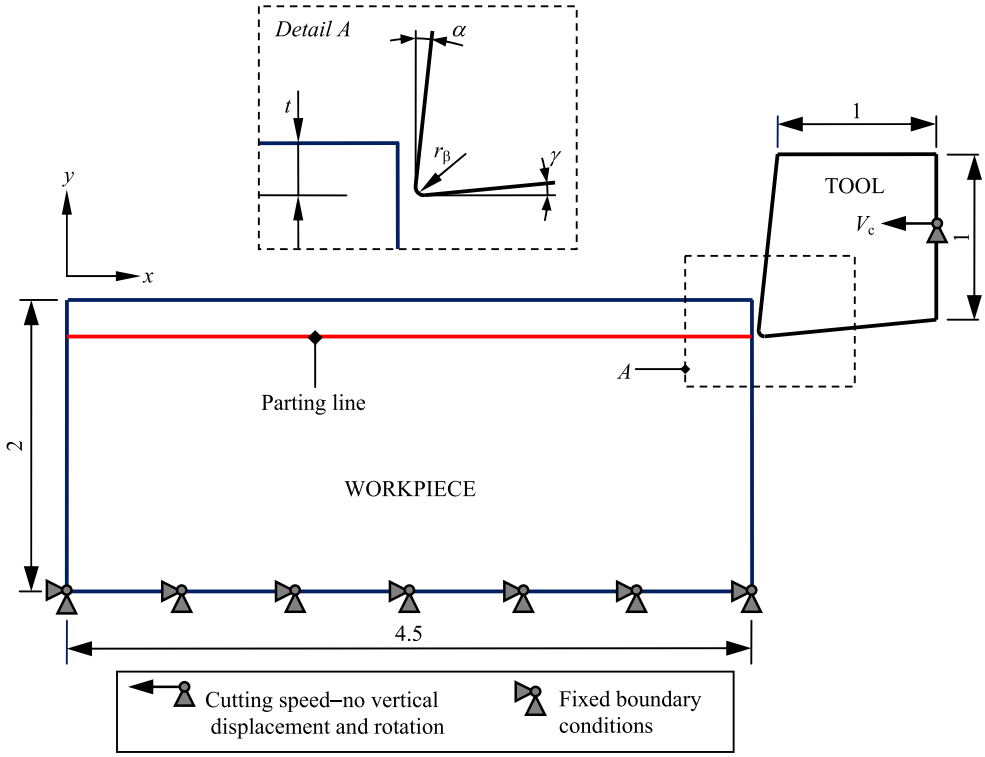

Fig. 1 ALE FE model with Lagrangian boundaries (dimensions in mm)

Where, $K_{tc,j,i}$, $K_{rc,j,i}$ and $K_{ac,j,i}$ represent the tangential, radial and axial instantaneous shearing force coefficients, respectively, and K_{te}, K_{re} and K_{ae} are the corresponding plowing force coefficients. $db_{j,i}$ is the chip width. $dS_{j,i}$ is the length of the curved cutting edge. The instantaneous undeformed chip thickness normal to the cutting edge is expressed as

$$t_{n,j,i}(\phi_{j,i},\kappa_{j,i}) = s_t \sin(\phi_{j,i}) \sin(\kappa_{j,i}) \tag{6}$$

Where, s_t is the feed rate per tooth and $\kappa_{j,i}=\sin^{-1}(r_{j,i}(\psi)/r_0)$ is the axial immersion angle. The radial immersion angle at axial depth z is calculated by

$$\phi_{j,i} = \phi + 2\pi(j\text{-}1)\Big/N_f - z \tan(\beta_0)\Big/r_0 \tag{7}$$

Where, j is the flute index and N_f is the number of flutes. ϕ is the rotation angle at axial depth $z=0$ of the reference flute ($j=1$).

The total X and Y cutting forces for the jth flute at a certain rotation angle ϕ are formulated as follows:

$$\begin{aligned} F_{x,j}(\phi) &= \int_{z_1}^{z_2}\Big[-dF_{r,j,i}\sin(\kappa_{j,i})\sin(\phi_{j,i}) - dF_{t,j,i}\cos(\phi_{j,i}) \\ &\quad - dF_{a,j,i}\cos(\kappa_{j,i})\sin(\phi_{j,i})\Big]\,dz_{j,i} \\ F_{y,j}(\phi) &= \int_{z_1}^{z_2}\Big[-dF_{r,j,i}\sin(\kappa_{j,i})\cos(\phi_{j,i}) + dF_{t,j,i}\sin(\phi_{j,i}) \\ &\quad - dF_{a,j,i}\cos(\kappa_{j,i})\cos(\phi_{j,i})\Big]\,dz_{j,i} \end{aligned} \tag{8}$$

Where, z_1 and z_2 are the lower and upper axial boundaries. Eventually, the contributions of the entire flutes are summed to find the total $F_x(\phi)$ and $F_y(\phi)$ at a rotation angle ϕ.

$$F_x(\phi) = \sum_{j=1}^{N_f} F_{x,j}(\phi) \quad F_y(\phi) = \sum_{j=1}^{N_f} F_{y,j}(\phi) \tag{9}$$

4 Determination of shearing and ploughing force coefficients

The average force-based method, the unified mechanics of cutting approach, has been used to establish the shearing and ploughing force coefficients [8]. On the other hand, Gonzalo et al. [28] presented a different approach to obtain the force coefficients from FE models without any experimental works. In the present study, a set of orthogonal cutting simulations was carried out at various undeformed chip thicknesses (t) and cutting speeds (V_c) but at constant depth of cut (a) to estimate the shearing and ploughing force coefficients. Then, the tangential force (F_t) and radial force (F_r) were determined from the orthogonal cutting simulations and expressed as follows:

$$\begin{aligned} F_t &= K_{tc}\ a\ t + K_{te}\ a \\ F_r &= K_{rc}\ a\ t + K_{re}\ a \end{aligned} \tag{10}$$

Where, K_{te} and K_{re} are calculated from the force axis intercept of the force-undeformed chip thickness functions, which are presented in Eq. (10). K_{ae} is taken as 0 in oblique cutting.

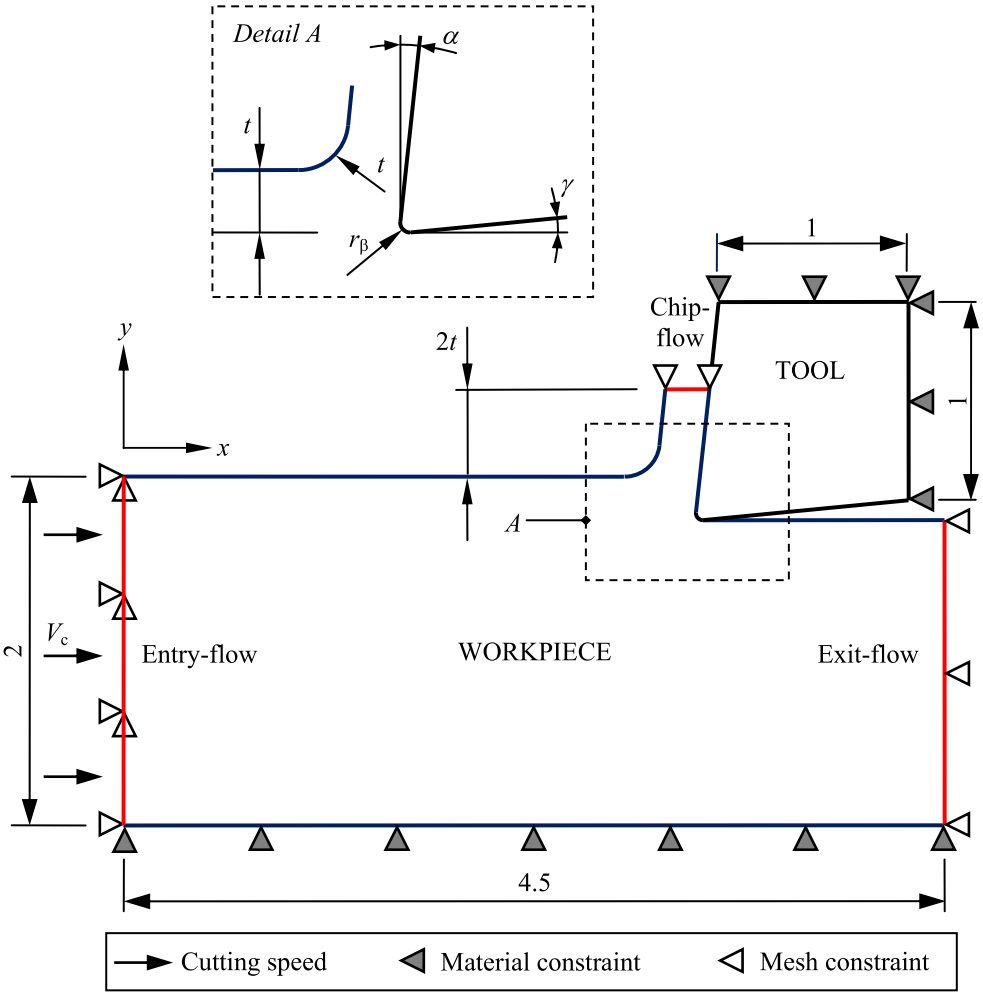

Fig. 2 ALE FE model using Eulerian–Lagrangian boundaries (dimensions in mm)

Because of the variation of $r_{j,i}(\psi)$, $\beta_{j,i}(\psi)$ and $\kappa_{j,i}$ at the hemispherical piece of the milling cutter, K_{tc}, K_{rc} and K_{ac} can be expressed by the instantaneous shearing force coefficients $K_{tc,j,i}$, $K_{rc,j,i}$ and $K_{ac,j,i}$ which are carried to oblique cutting edge geometry by utilizing the following oblique transformation model and the orthogonal cutting data:

$$\begin{aligned} K_{tc,j,i} &= \left[\left(\frac{\tau_s}{\sin(\phi_{n,j,i})}\right)\left(\frac{\cos(\beta_{n,j,i}-\alpha_{n,j,i}(\psi)) + \tan(\eta_c)\sin(\beta_{n,j,i})\tan(\beta_{j,i}(\psi))}{c}\right)\right] \\ K_{rc,j,i} &= \left[\left(\frac{\tau_s}{\sin(\phi_{n,j,i})\cos(\beta_{j,i}(\psi))}\right)\left(\frac{\sin(\beta_{n,j,i}-\alpha_{n,j,i}(\psi))}{c}\right)\right] \\ K_{ac,j,i} &= \left[\left(\frac{\tau_s}{\sin(\phi_{n,j,i})}\right)\left(\frac{\cos(\beta_{n,j,i}-\alpha_{n,j,i}(\psi))\tan(\beta_{j,i}(\psi)) - \tan(\eta_c)\sin(\beta_{n,j,i})}{c}\right)\right] \end{aligned} \quad (11)$$

where,

$$c = \sqrt{\cos^2(\phi_{n,j,i}+\beta_{n,j,i}-\alpha_{n,j,i}(\psi)) + \tan^2(\eta_c)\sin^2(\beta_{n,j,i})}.$$

where τ_s is the shear stress in the shear plane. For simplicity in Eq. (11), the Stabler rule [29] is used in which the chip flow angle (η_c) is assumed to be equal to $\beta_{j,i}(\psi)$. $\beta_{n,j,i}$ and $\phi_{n,j,i}$ are the friction and shear angles in the normal plane, respectively.

The normal rake angle along the hemispherical piece of the milling cutter ($\alpha_{n,j,i}(\psi)$) can be found by [8]:

$$\tan(\alpha_{n,j,i}(\psi)) = \tan(\alpha_{r,j,i}(\psi))\cos(\beta_{j,i}(\psi)) \quad (12)$$

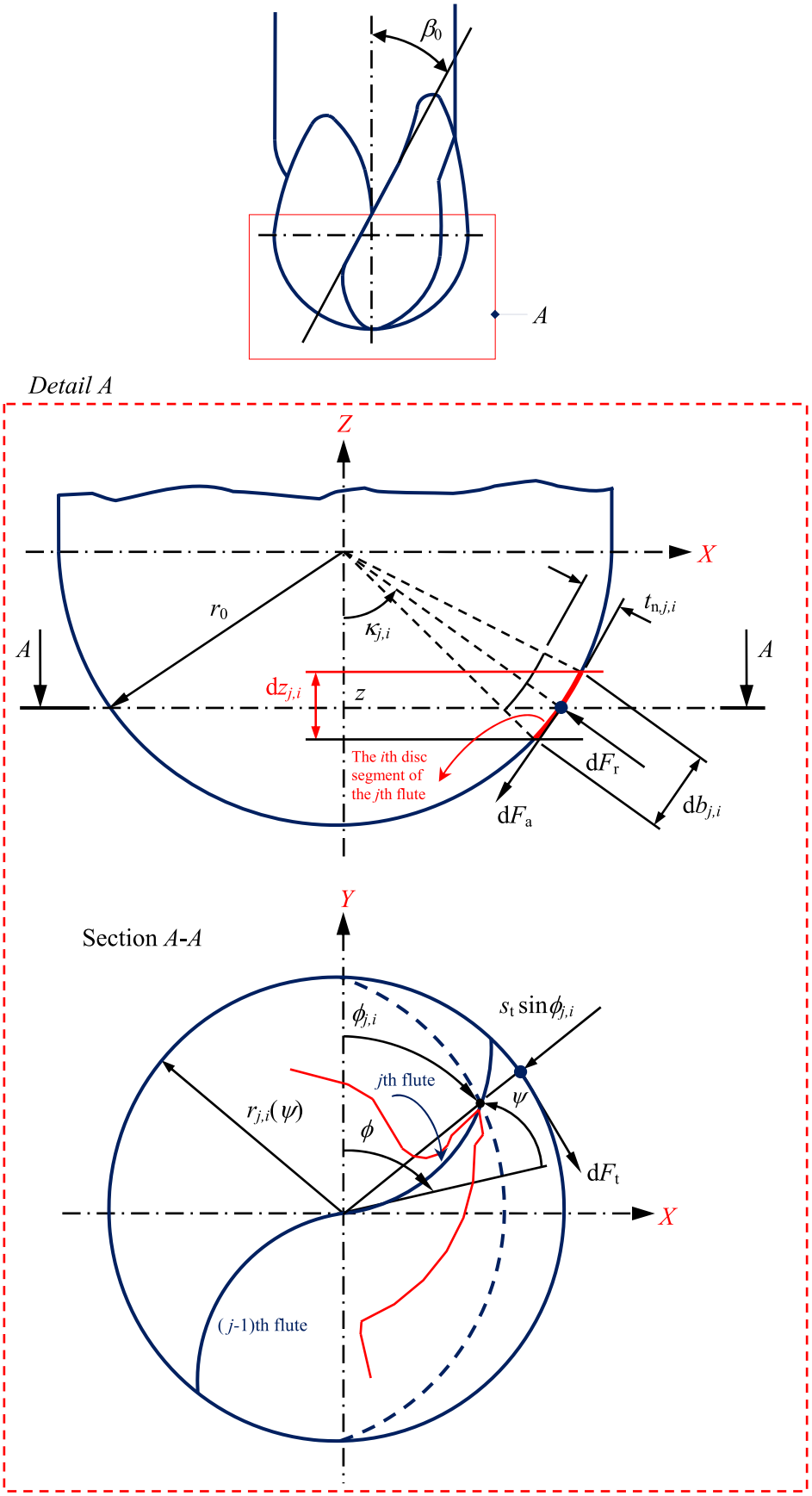

Fig. 3 Cutting forces and geometry of the ball-end milling cutter

Where, the radial rake angle along the hemispherical piece ($\alpha_{r,j,i}(\psi)$) varies as follows: [30]

$$\alpha_{r,j,i}(\psi) = \begin{cases} \alpha_r \sin(\kappa_{j,i}) & 0 \le z < r_0 \\ \alpha_r & z \ge r_0 \end{cases} \quad (13)$$

Where, α_r is the radial rake angle of the cylindrical piece of the milling cutter.

5 Results and discussion

5.1 Analysis of orthogonal cutting data

To study the effect of ALE FE models on the estimation accuracy of ball-end milling forces, numerical simulations have been conducted. The von Mises stress (σ_{vM}) was studied to carefully select an appropriate mesh size for the numerical simulations. Figures 4 and 5 show typical examples of the σ_{vM} distribution in the workpiece for the ALE FE models. A high-stress field due to shearing was achieved in the primary shear zone extending from the tool tip to the free surface. The stress resulting from additional shearing in the secondary deformation zone was lower than that in the primary deformation zone.

As discussed earlier, this study deals with the formation of a continuous chip. The mesh size in the chip was varied by considering meshx1, meshx2 and meshx3 values in the chip thickness direction. As shown in Fig. 4a and b, the ALE FE simulations with Lagrangian boundaries were carried out without severe mesh distortion using meshx1 and meshx2 values. In case of meshx3 with a finer mesh size, the ALE FE simulation with Lagrangian boundaries was unable to run beyond 4.5×10^{-4} s since a high mesh distortion was generated during the cutting process, as seen in Fig. 4c. The ALE FE simulations with Eulerian–Lagrangian boundaries were successfully carried out at all the mesh sizes, as seen in Fig. 5. Table 4 shows the σ_{vM} values obtained in a thin layer near the tool/chip interface of the sticking region for both ALE

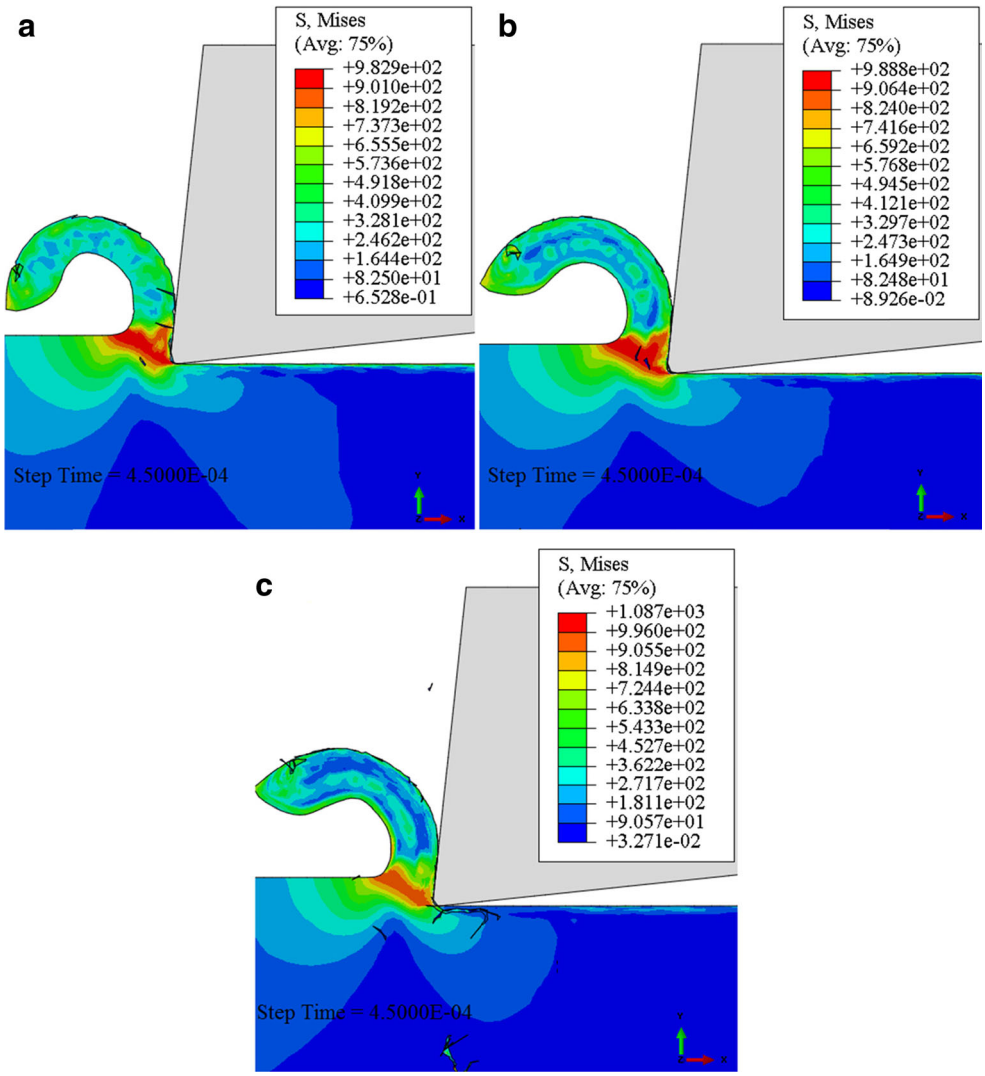

Fig. 4 The σ_{vM} distribution estimated from the ALE FE model with Lagrangian boundaries (V_c = 3.5 m/s, t = 0.1 mm): **a** meshx1, **b** meshx2 and **c** meshx3

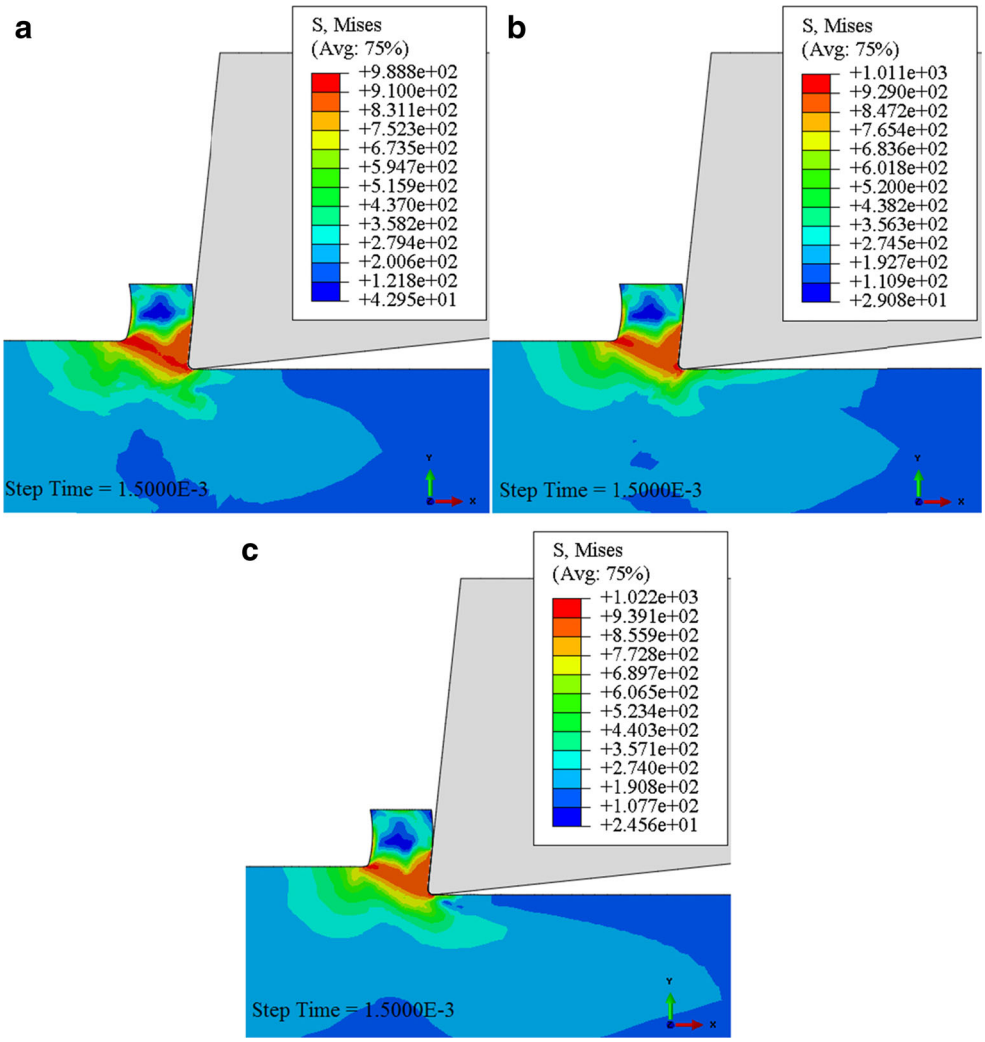

Fig. 5 The σ_{vM} distribution estimated from the ALE FE model with Eulerian–Lagrangian boundaries (V_c = 3.5 m/s, t = 0.1 mm): **a** meshx1, **b** meshx2 and **c** meshx3

FE models. In the ALE FE simulations with Lagrangian boundaries, the meshx2 provided the lower stress value than that obtained from the meshx1. This difference can be the consequence of a finer mesh size. From the ALE FE simulations with Eulerian–Lagrangian boundaries using three different mesh sizes, it was found that there was a slight difference among the stress values. When the stress values calculated from each ALE FE model were also compared, it was determined that the ALE FE model with Eulerian–Lagrangian boundaries caused higher stress values since the stress distribution was more concentrated along the shear plane. Based on the obtained results, it can be deduced that the meshx2 with an element size varying from 2.5×10^{-3} to 5×10^{-3} mm was more suitable for the ALE FE simulations. Therefore, the orthogonal cutting data were determined using the meshx2 value.

The ALE FE simulations were carried out in a 2.6 GHz computer with 8 GB RAM. Table 4 shows the variations of the

Table 4 Computational time and σ_{vM} values obtained in the FE simulations

Model	Mesh size	Simulation time (s)	Computational time (h:min:s)	σ_{vM} (MPa)
ALE FE model with Lagrangian boundaries	meshx1	1×10^{-3}	00:49:21	683
	meshx2	1×10^{-3}	01:16:36	566
	meshx3	1×10^{-3}	Simulation failed	–
ALE FE model with Eulerian–Lagrangian boundaries	meshx1	2.5×10^{-3}	00:59:33	911
	meshx2	2.5×10^{-3}	02:06:59	915
	meshx3	2.5×10^{-3}	11:18:25	917

computational time with respect to the simulation time for the ALE FE models and mesh sizes. It can be observed that the computational time increases with decreasing mesh size. In the ALE FE simulation with Lagrangian boundaries using the meshx2 value, the computational time was achieved as 1 h 16 min 36 s. When used, the ALE FE model with Eulerian–Lagrangian boundaries, the computational time reached 2 h 6 min 59 s due to modeling based on the Eulerian–Lagrangian boundaries.

From the simulations, the chip thickness (t_c) and the forces in the x and y directions, which correspond to F_t and F_r, respectively, were fundamentally estimated. These estimated variables were used to calculate the orthogonal cutting data. Figure 6 illustrates the convergence histories of the cutting forces at $V_c = 3.5$m/s and $t = 0.125$mm. The simulation times were determined by considering the stable range of the cutting forces since the transient forces occurred during the chip formation. The force patterns obtained from each ALE FE model were considerably different from each other in both magnitude and nature. This implied that the boundaries of the established ALE FE models affected the estimated force distributions. From the force variations in Fig. 6a achieved by implementing the ALE technique with Lagrangian boundaries, the average F_t and F_r were found as 614.8 and 118.1 N, respectively. By utilizing the ALE technique with Eulerian–Lagrangian boundaries, the average F_t and F_r were calculated as 702.4 and 179.5 N from the force distributions in Fig. 6b, respectively. When the cutting forces estimated from the ALE technique with Lagrangian boundaries were compared to those from the ALE technique with Eulerian–Lagrangian boundaries, the lower average force values were achieved by implementing the ALE technique with Lagrangian boundaries. This magnitude difference would mainly affect the plowing force parts ($K_{te}dS_{j,i}$, $K_{re}dS_{j,i}$) of the force model in Eq. (5).

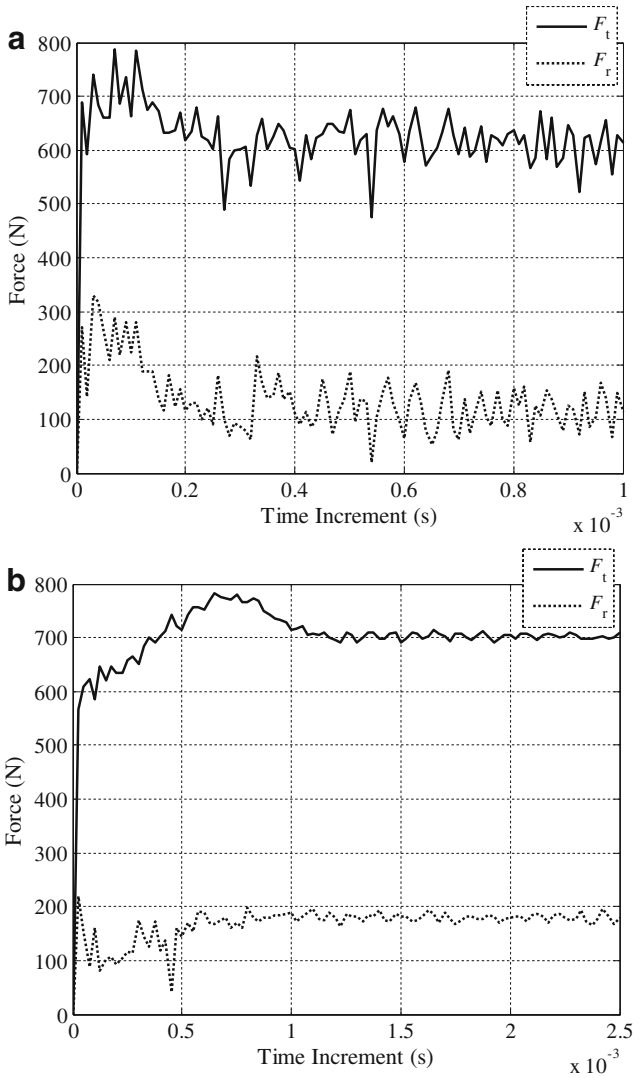

Fig. 6 Time histories of the cutting forces for the ALE FE models: **a** Lagrangian and **b** Eulerian–Lagrangian boundaries

Figures 7 and 8 show F_t and F_r versus the undeformed chip thickness for each ALE technique. A linear relationship between the forces and undeformed chip thickness was achieved by curve fitting to the orthogonal cutting forces. Also, the ploughing forces did not change considerably with increasing cutting speed for 20NiCrMo5 steel. This means that average values of the ploughing force coefficients can be treated in the analysis.

The average and the standard deviation of the ploughing force coefficients found from the ALE technique with Lagrangian boundaries were $K_{te} = 19.74$ N/mm with $\sigma(K_{te}) = 1.8$ and $K_{re} = 23.07$ N/mm with $\sigma(K_{re}) = 1.66$, respectively. Using the ALE technique with Eulerian–Lagrangian boundaries, the average and the standard deviation of the ploughing force coefficients were achieved as $K_{te} = 25.18$ N/mm with $\sigma(K_{te}) = 2.19$ and $K_{re} = 38.47$ N/mm with $\sigma(K_{re}) = 4.52$, respectively. When the ploughing force

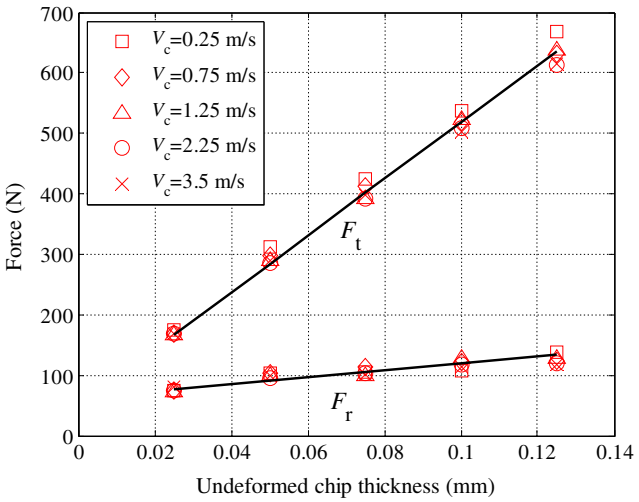

Fig. 7 The estimated F_t and F_r from the ALE technique with Lagrangian boundaries

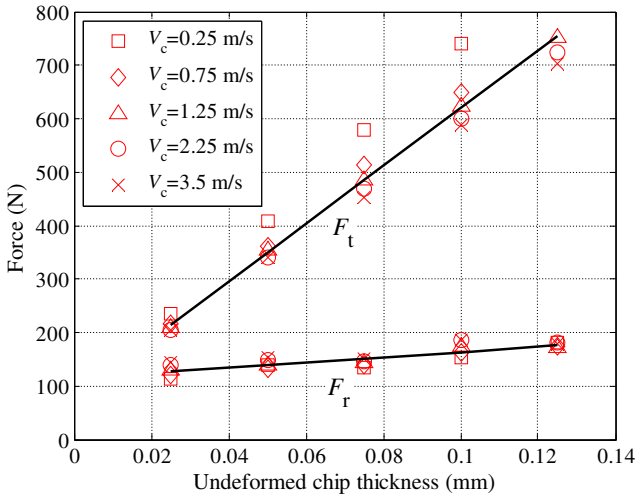

Fig. 8 The estimated F_t and F_r from the ALE technique with Eulerian–Lagrangian boundaries

coefficients achieved from the simulations using two different approaches were compared, there were significant differences between the coefficients obtained from the ALE technique with Lagrangian boundaries and those estimated by the ALE technique with Eulerian–Lagrangian boundaries. The differences were −5.44 N/mm (−21.6%) in K_{te} and −15.4 N/mm (−40%) in K_{re}. Obviously, the boundaries of the ALE FE models change the ploughing force coefficients.

Figure 9 shows the variation tendency of the chip thickness ratio in orthogonal cutting (r_c) with the V_c and ALE techniques. As it can be seen from the figure, r_c exponentially varies with V_c for 20NiCrMo5 steel and was defined as exponential functions of V_c for both the ALE techniques as follows:

$$r_c = \begin{cases} 0.7382 \;\; V_c^{\,0.0503} & \text{(Lagrangian)} \\ 0.4684 \;\; V_c^{\,0.11} & \text{(Eulerian-Lagrangian)} \end{cases} \tag{14}$$

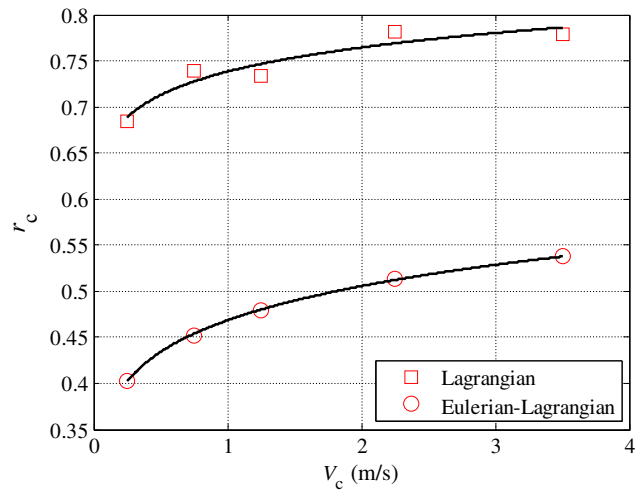

Fig. 9 Variation of r_c in orthogonal cutting simulations

The shear stress in the shear plane (τ_s) and friction angle at the rake face (β_a) were estimated by applying the orthogonal cutting theory introduced in Ref. [8]. The identified values are presented in Table 5. τ_s and β_a slightly change with V_c for each ALE FE model. The slight variation in τ_s can be attributed to the opposite influences of the heat and the strain rate in the primary shear zone. In other words, after the material is deformed in the primary shear zone, the high values of the strain rate occur and the shear stress significantly increases with the strain rate. High cutting speed also causes low stress values in the primary shear zone.

Based on the above explanation, average values were determined for τ_s and β_a. From the ALE technique with Lagrangian boundaries, the average value and percentage difference of τ_s and β_a were calculated as $\tau_s = 685.6$ MPa with $\varepsilon(\tau_s) = 1.71$ and $\beta_a = 25.6^\circ$ with $\varepsilon(\beta_a) = 0.98$, respectively. Using the ALE technique with Eulerian–Lagrangian boundaries, the average value and percentage difference of τ_s and β_a were found as $\tau_s = 700.3$ MPa with $\varepsilon(\tau_s) = 3.69$ and $\beta_a = 29.3^\circ$ with $\varepsilon(\beta_a) = 7.43$, respectively. Consequently, the average τ_s and β_a found by the ALE technique using Eulerian–Lagrangian boundaries were slightly larger than those obtained from the ALE technique using Lagrangian boundaries. It can be noted that τ_s and β_a correspond to the flow stress ($\overline{\sigma}$) and the friction coefficients (μ), respectively, which are presented in "Section 2." That is, the FE modeling of the orthogonal cutting process can be implemented to determine the flow stress and the friction at the tool/chip interface for machining conditions.

5.2 Simulation and experimental verification

The ball-end milling experiments have been conducted for analyzing the capabilities of the presented ALE FE models by comparing the measurements with the estimations achieved by numerical integration of Eq. (8). The milling experiments were performed on 20NiCrMo5 steel without

Table 5 τ_s and β_a estimated from cutting simulations

Model	V_c (m/s)	τ_s (MPa)	β_a (°)
ALE FE model with Lagrangian boundaries	0.25	710.2	25.0
	0.75	690.6	25.9
	1.25	673.4	25.6
	2.25	674.8	25.5
	3.5	679.2	25.8
	Average	685.6	25.6
ALE FE model with Eulerian–Lagrangian boundaries	0.25	756.9	25.4
	0.75	709.2	27.8
	1.25	690.0	29.6
	2.25	675.5	31.4
	3.5	669.9	32.2
	Average	700.3	29.3

lubrication for three different cutting speeds $V_c = 1$, 2 and 3 m/s and feed rates $s_t = 0.025$, 0.05 and 0.075 mm/flute at the axial depth of cut $a_p = 3$ mm. The entry angle was $\phi_{st} = 0^\circ$ and the exit angle was defined by $\phi_{ex} = \pi$. The cutting tools were two-fluted carbide milling cutters with helix angle $\beta_0 = 30^\circ$, the radial rake angle $\alpha_r = 7^\circ$, the normal rake angle $\alpha_n = 6^\circ$ and radius $r_0 = 6$ mm. The forces, namely F_x and F_y, were recorded by a Kistler dynamometer (9257B) on a Quaser MV154C three-axis vertical machining center. The experimental setup is presented in Fig. 10.

The ploughing force coefficients K_{te} and K_{re} were calculated from the orthogonal cutting simulations and remained constant for all milling simulations. The shearing force coefficients $K_{tc,j,i}$, $K_{rc,j,i}$ and $K_{ac,j,i}$ were calculated using Eq. (11) with τ_s, β_a, r_c and η_c. Figures 11, 12 and 13 show the variations of the shearing force coefficients $K_{tc,j,i}$, $K_{rc,j,i}$ and $K_{ac,j,i}$ with a_p. The coefficients which were estimated from the ALE technique with Lagrangian boundaries are given in Figs. 11a, 12a and 13a. The results obtained by applying the ALE technique with Eulerian–Lagrangian boundaries are presented in Figs. 11b, 12b and 13b. It was observed that the estimated coefficients $K_{tc,j,i}$, $K_{rc,j,i}$ and $K_{ac,j,i}$ were not constant along a_p since they depend on $\beta_{j,i}(\psi)$ which varies from the nominal value to zero along the hemispherical piece. $K_{tc,j,i}$ and $K_{rc,j,i}$ mostly revealed a decrease with an increase in a_p while an increase of a_p caused a rising trend on $K_{ac,j,i}$.

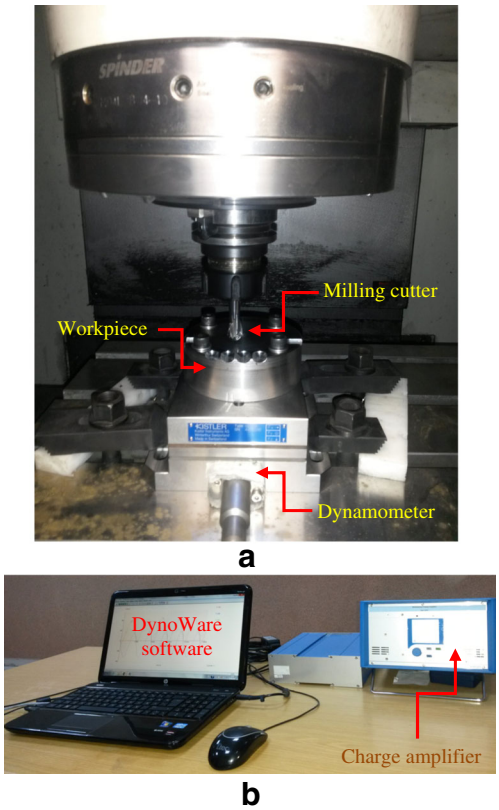

Fig. 10 Experimental setup. **a** Workpiece mounted on the dynamometer. **b** Charge amplifier and DynoWare software

The relative differences between the coefficient values were computed to investigate the effect of the ALE techniques on $K_{tc,j,i}$, $K_{rc,j,i}$ and $K_{ac,j,i}$. The results showed that the lowest relative differences between the estimations of the different ALE techniques were −3.4, −18.1 and 10.7% at $V_c = 1$ m/s for the coefficients $K_{tc,j,i}$, $K_{rc,j,i}$ and $K_{ac,j,i}$, respectively. At $V_c = 2$ m/s, the lowest relative differences of the coefficients $K_{tc,j,i}$, $K_{rc,j,i}$ and $K_{ac,j,i}$ were found to be −2.8, −17.6 and 11.1%, respectively. At $V_c = 3$ m/s, the lowest relative differences of the coefficients $K_{tc,j,i}$, $K_{rc,j,i}$ and $K_{ac,j,i}$ decreased to −2.6, −17.4 and 11%, respectively. Besides, the greatest relative differences of the estimated coefficients $K_{tc,j,i}$, $K_{rc,j,i}$ and $K_{ac,j,i}$ from the different ALE techniques reached −4.8, −19.2 and 14.3% at $V_c = 1$ m/s, respectively. At $V_c = 2$ m/s, the greatest relative differences of the coefficients $K_{tc,j,i}$, $K_{rc,j,i}$ and $K_{ac,j,i}$ were −4.1, −18.7 and 15.3% respectively. At $V_c = 3$ m/s, the greatest relative differences of the coefficients $K_{tc,j,i}$, $K_{rc,j,i}$ and $K_{ac,j,i}$ were found to be −4.2, −18.8 and 15.6%, respectively. It can be concluded that the relative differences between the coefficients $K_{tc,j,i}$ estimated from the two different ALE techniques were lesser than 5%. The relative differences between the coefficients $K_{rc,j,i}$ obtained from the ALE technique with Lagrangian boundaries and the ALE technique with Eulerian–Lagrangian boundaries were as high as about 20% for three different cutting speeds. The relative discrepancies between the estimated coefficients $K_{ac,j,i}$ were approximately within 11–16%. Consequently, the coefficients $K_{tc,j,i}$ estimated with the different ALE techniques were close to each other, but the coefficients $K_{rc,j,i}$ and $K_{ac,j,i}$ obtained from both the ALE techniques were relatively different.

Table 6 shows the comparisons between the estimated and measured average forces. The absolute percentage deviation between the average values of the estimations and measurements has been used for evaluating the performance of the FE models. There were notable discrepancies between the estimated outcomes from both models. When using the predictive cutting force model with orthogonal cutting data based on the ALE technique using Lagrangian boundaries, the mean absolute deviations of the estimated F_x and F_y were found as 21.6 and 24.6%, respectively. The highest percentage deviation obtained was lesser than 30% for the estimated forces. The mean absolute deviations of the estimated F_x and F_y based on the predictive force model with orthogonal cutting data identified from the ALE technique using Eulerian–Lagrangian boundaries were 9.9 and 12.6%, respectively. The highest percentage deviation obtained was lesser than 20% for the estimated forces, apart from Test 9. It can be seen from the results that the estimated forces based on the predictive force model with orthogonal cutting data identified from the ALE technique using Eulerian–Lagrangian boundaries were closer to the measured forces when compared with those obtained by

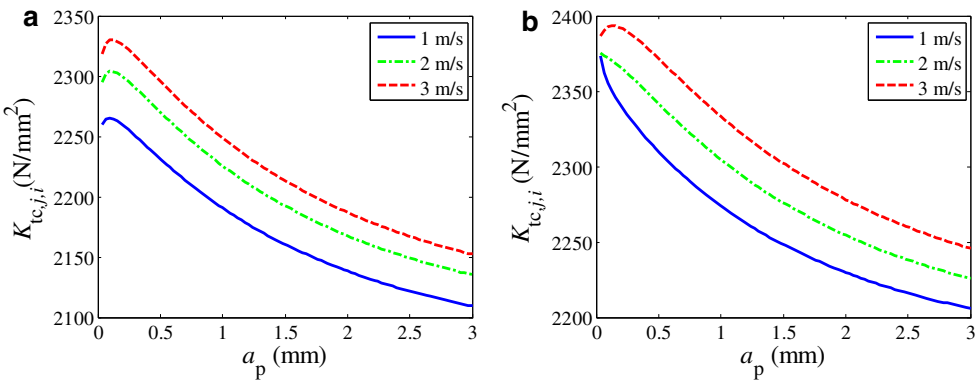

Fig. 11 Estimated coefficient $K_{tc,j,i}$. **a** Lagrangian. **b** Eulerian–Lagrangian boundaries

the force model with orthogonal cutting data based on the ALE technique with Lagrangian boundaries.

The estimated and measured instantaneous F_x and F_y profiles have also investigated to see the effectiveness of the ALE FE models. Figure 14 shows the estimated and measured F_x and F_y variations in slot-milling operation at $V_c = 1$ m/s and $s_t = 0.075$ mm/flute. In the force model with orthogonal cutting data determined numerically from the ALE technique with Eulerian–Lagrangian boundaries, the percentage deviation and accuracy were found as about 18 and 82% for both the average F_x and F_y, respectively. When using the predictive force model based on the ALE technique with Lagrangian boundaries, the discrepancy between the estimated and measured data reached up to 29.8% for average F_x and 27.6% for average F_y. Although the same workpiece and tool properties were used for both the FE models, the deviations between the outcomes obtained from experiment and estimated by the ALE technique with Lagrangian boundaries were relatively large, and also the estimated forces did not match exactly with the measured forces through rotation angle.

In Fig. 15, the estimated and measured F_x and F_y variations for slot-milling operation with feed rate $s_t = 0.05$ mm/flute at $V_c = 2$ m/s are shown. The predictive cutting force model with orthogonal cutting data based on the ALE technique using Eulerian–Lagrangian boundaries produced a relatively low deviation of 6.9% for average F_x while a discrepancy of 13% between the estimations and measurements was found for average F_y. Further, the estimated and measured waveforms were highly consistent in the pattern and magnitude. In the predictive force model with orthogonal cutting data evaluated from the ALE technique using Lagrangian boundaries, the corresponding values in the percentage deviation increased by 21.4% for average F_x and 24.2% for average F_y. In other words, there were clear differences between the estimations and measurements in terms of the peak values and patterns. It can be clearly inferred from the obtained outcomes that the predictive cutting force approach along with the ALE technique with Eulerian–Lagrangian boundaries provides quite a high accuracy.

As seen in Fig. 16, in case of a slot-milling operation with $V_c = 3$ m/s and $s_t = 0.025$ mm/flute, the cutting force patterns, which were extracted from the predictive force approach based on the ALE technique using Eulerian–Lagrangian boundaries, were substantially close to the experimental ones. The values in percentage deviation for average F_x and F_y were 4.7 and 2.3%, respectively. That is, the estimation accuracies were as high as 95.3 and 97.7% for average F_x and F_y,

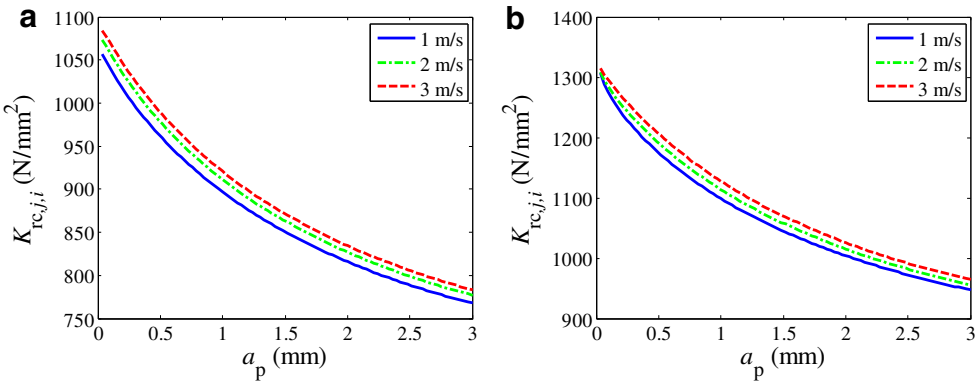

Fig. 12 Estimated coefficient $K_{rc,j,i}$. **a** Lagrangian. **b** Eulerian–Lagrangian boundaries

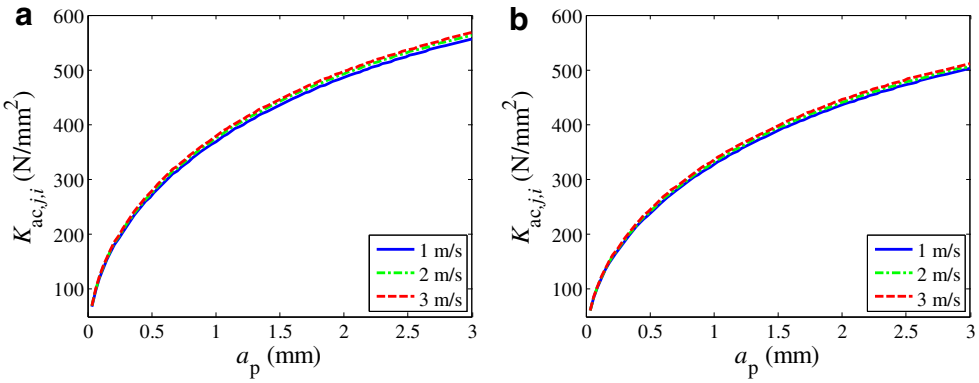

Fig. 13 Estimated coefficient $K_{ac,j,i}$. **a** Lagrangian. **b** Eulerian–Lagrangian boundaries

respectively. It can be deduced that the results estimated from the predictive approach with orthogonal cutting quantities based on the ALE technique with Eulerian–Lagrangian boundaries closely match with those obtained experimentally. In the predictive approach with machining parameters determined from the ALE technique with Lagrangian boundaries, the discrepancy between the estimated and measured data was found as 15.8% for average F_x and 18.8% for average F_y. Obviously, these results were far from the obtained data by the former approach.

In summary, it was found that the accuracy of the force estimations computed by using the ALE technique with Eulerian–Lagrangian boundaries was higher than the accuracy obtained by the ALE technique with Lagrangian boundaries. This difference observed between both the ALE techniques can be attributed to the variation in the boundary conditions within the chip region. Using the unified mechanics of the cutting approach, the estimated milling forces can be achieved closer to the measured results because the higher stress values were generated along the primary shear zone

Table 6 Comparison of estimated and measured F_x and F_y

Test no	Cutting speed V_c, m/s	Feed per tooth f_t, mm/flute	Force direction	Measured force, N	Lagrangian		Eulerian-Lagrangian	
					Predicted force, N	Deviation ε, %	Predicted force, N	Deviation ε, %
1	1	0.025	F_x	160.0	137.6	14.0	171.7	7.3
			F_y	216.6	164.0	24.3	198.0	8.6
2	1	0.05	F_x	251.9	194.4	22.8	231.1	8.3
			F_y	330.1	244.8	25.8	281.7	14.7
3	1	0.075	F_x	357.9	251.4	29.8	290.9	18.7
			F_y	450.2	325.8	27.6	365.7	18.8
4	2	0.025	F_x	163.7	138.5	15.4	172.4	5.3
			F_y	206.8	165.2	20.1	198.9	3.8
5	2	0.05	F_x	249.6	196.1	21.4	232.4	6.9
			F_y	326.1	247.3	24.2	283.7	13.0
6	2	0.075	F_x	351.0	253.9	27.7	293.0	16.5
			F_y	440.9	329.4	25.3	368.7	16.4
7	3	0.025	F_x	165.2	139.1	15.8	173.0	4.7
			F_y	204.5	166.0	18.8	199.8	2.3
8	3	0.05	F_x	254.4	197.2	22.5	233.8	8.1
			F_y	334.2	248.8	25.6	285.5	14.6
9	3	0.075	F_x	339.5	255.6	24.7	294.9	13.1
			F_y	469.9	331.8	29.4	371.4	21.0
Mean absolute deviation	F_x			21.6		9.9		
	F_y			24.6		12.6		

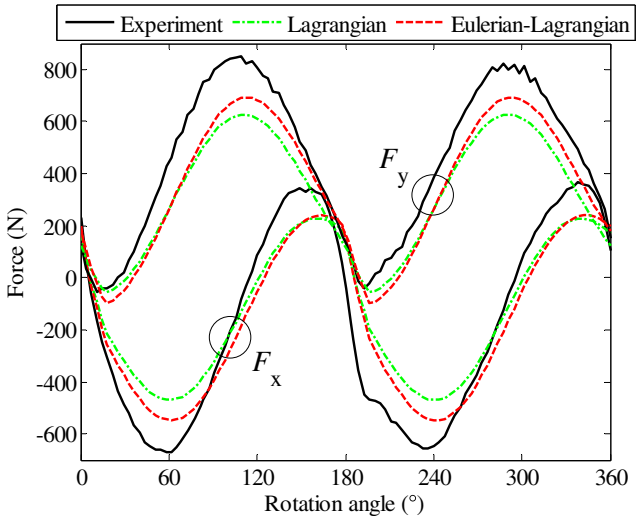

Fig. 14 Estimated and measured F_x and F_y in slot milling at V_c = 1 m/s, s_t = 0.075 mm/flute

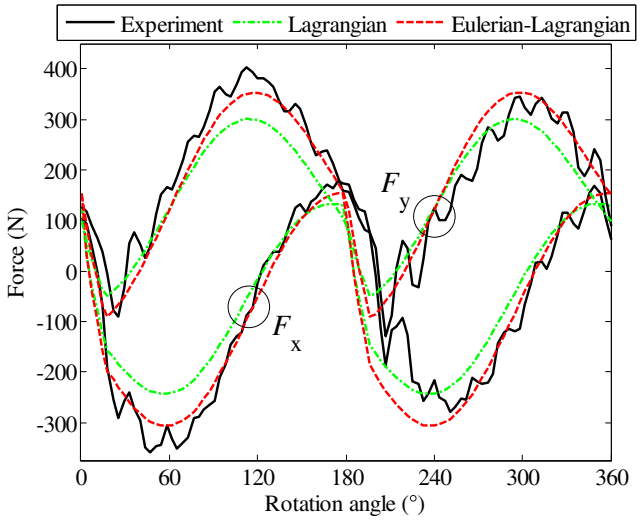

Fig. 16 Estimated and measured F_x and F_y in slot milling at V_c = 3 m/s, s_t = 0.025 mm/flute

in the ALE FE model with Eulerian-Lagrangian boundaries. In addition, when the feed rate was increased from 0.025 to 0.075 mm/flute at the same cutting speed for each ALE technique, higher deviations were found. It is evident that the feed rate is a critical parameter for higher accuracy in the estimation of ball-end milling forces. From these results, it can be deduced that the orthogonal cutting data can be calculated with a satisfactory accuracy by applying the ALE technique with Eulerian–Lagrangian boundaries. The predictive force model along with the identified orthogonal cutting data can be utilized for estimating the ball-end milling forces at different cutting speed, feed rate and depth of cut conditions. This signifies that the ALE technique with Eulerian–Lagrangian boundaries is greatly useful in eliminating the expense of experimental operations.

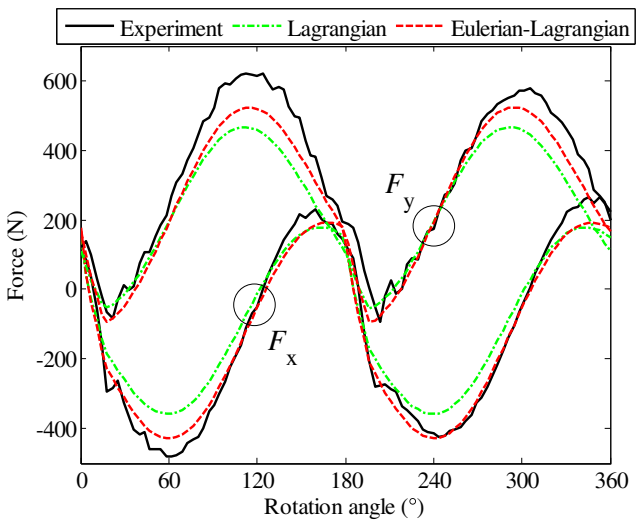

Fig. 15 Estimated and measured F_x and F_y in slot milling at V_c = 2 m/s, s_t = 0.05 mm/flute

6 Conclusions

The presented work emphasizes the significance of ALE techniques to more accurately estimate fundamental cutting quantities from FE modeling of the chip formation process for estimating the cutting forces in ball-end milling. Two different models to establish a more realistic database of cutting parameters such as τ_s, β_a and r_c have been proposed: ALE technique with Lagrangian boundaries and ALE technique with Eulerian–Lagrangian boundaries. The following points can be concluded:

- An obvious knowledge of ALE FE simulations of the machining process was provided and the information about the cutting parameters such as τ_s, β_a and r_c for machining of 20NiCrMo5 material with tungsten carbide tool was advanced.
- Comparing the estimated cutting forces with experimental data, it was found that the unified mechanics of the cutting approach with the ALE technique using Eulerian–Lagrangian boundaries decreased the deviation up to about 5 and 3% for average F_x and F_y, respectively. To estimate the accurate cutting forces, the capability of the ALE technique with Eulerian–Lagrangian boundaries was better than the ALE technique using Lagrangian boundaries.
- The unified mechanics of cutting approach indicated that the ball-end milling forces were more correctly captured by the ploughing and shearing force coefficients obtained from the ALE technique using Eulerin–Lagrangian boundaries.
- When the cutting speed was kept constant in slot milling with the ball-end milling cutter, the predictive force model based on the ALE FE models produced higher deviations

as the feed rate increased. Accordingly, the cutting parameters have a critical significance on the accuracy of the ball-end milling force estimations.

- Experimentally, it is very costly to determine orthogonal cutting data. The obtained results revealed that the ALE FE model with Eulerian–Lagrangian boundaries can be adopted as an alternative tool in producing a cutting database with a satisfactory accuracy.

References

1. Hosseini A, Imani BM, Kishawy HA (2011) Mechanistic modelling for cutting with serrated end mills—a parametric representation approach. Proc I MechE, Part B: J Engineering Manufacture 225:1019–1032
2. Wan M, Zhang WH, Tan G, Qin GH (2007) New algorithm for calibration of instantaneous cutting-force coefficients and radial run-out parameters in flat end milling. Proc I MechE, Part B: J Engineering Manufacture 221:1007–1019
3. Srinivasa YV, Shunmugam MS (2013) Mechanistic model for prediction of cutting forces in micro end-milling and experimental comparison. Int J Mach Tools Manuf 67:18–27
4. Aydın M, Uçar M, Cengiz A, Kurt M, Barkın B (2014) A methodology for cutting force prediction in side milling. Mater Manuf Process 29:1429–1435
5. Aydın M, Uçar M, Cengiz A, Kurt M (2015) Identification of static surface form errors from cutting force distribution in flat-end milling processes. J Braz Soc Mech Sci 37:1001–1013
6. Fernández-Abia AI, García JB, López de Lacalle LN, Neto OP (2014) Estimation of cutting forces and tool wear using modified mechanistic models in high performance turning. In: Davim JP (ed) Traditional machining processes: research advances, 1st edn. Springer-Verlag, Heidelberg, pp 49–107
7. Uriarte L, Azcárate S, Herrero A, Lopez de Lacalle LN, Lamikiz A (2008) Mechanistic modelling of the micro end milling operation. Proc I MechE, Part B: J Engineering Manufacture 222:23–33
8. Budak E, Altintas Y, Armarego EJA (1996) Prediction of milling force coefficients from orthogonal cutting data. Trans ASME J Manuf Sci Eng 118:216–224
9. Wan M, Pan WJ, Zhang WH, Ma YC, Yang Y (2014) A unified instantaneous cutting force model for flat end mills with variable geometries. J Mater Process Technol 214:641–650
10. Lee P, Altıntaş Y (1996) Prediction of ball-end milling forces from orthogonal cutting data. Int J Mach Tools Manuf 36:1059–1072
11. Wei ZC, Wang MJ, Cai YJ, Wang SF (2013) Prediction of cutting force in ball-end milling of sculptured surface using improved Z-map. Int J Adv Manuf Technol 68:1167–1177
12. Cao Q, Zhao J, Li Y, Zhu L (2013) The effects of cutter eccentricity on the cutting force in the ball-end finish milling. Int J Adv Manuf Technol 69:2843–2849
13. Saffar RJ, Razfar MR, Zarei O, Ghassemieh E (2008) Simulation of three-dimension cutting force and tool deflection in the end milling operation based on finite element method. Simul Model Pract Th 16:1677–1688
14. Prasad CS (2010) FEM modeling to verify residual stress in orthogonal machining. Lap Lambert Academic Publishing, Saarbrücken
15. Miguélez MH, Soldani X, Molinari A (2013) Analysis of adiabatic shear banding in orthogonal cutting of Ti alloy. Int J Mech Sci 75:212–222
16. Duan C, Zhang L (2013) A reliable method for predicting serrated chip formation in high-speed cutting: analysis and experimental verification. Int J Adv Manuf Technol 64:1587–1597
17. Ye GG, Chen Y, Xue SF, Dai LH (2014) Critical cutting speed for onset of serrated chip flow in high speed machining. Int J Mach Tools Manuf 86:18–33
18. Ducobu F, Rivière-Lorphèvre E, Filippi E (2014) Numerical contribution to the comprehension of saw-toothed Ti6Al4V chip formation in orthogonal cutting. Int J Mech Sci 81:77–87
19. Zhang Y, Umbrello D, Mabrouki T, Rizzuti S, Nelias D, Gong Y (2013) On different FE-based models to simulate cutting operation of titanium alloy (Ti-6Al-4V). Mechanika 19:349–357
20. Strenkowski JS, Shih AJ, Lin JC (2002) An analytical finite element model for predicting three-dimensional tool forces and chip flow. Int J Mach Tools Manuf 42:723–731
21. Raczy A, Altenhof WJ, Alpas AT (2004) An Eulerian finite element model of the metal cutting process. In Proceedings of the 8th International LS-DYNA Users Conference, Dearborn, MI, USA, pp 11–26
22. Arrazola PJ, Özel T (2010) Investigations on the effects of friction modeling in finite element simulation of machining. Int J Mech Sci 52:31–42
23. Adetoro OB, Wen PH (2010) Prediction of mechanistic cutting force coefficients using ALE formulation. Int J Adv Manuf Technol 46:79–90
24. Aydin M (2017) Prediction of cutting speed interval of diamond-coated tools with residual stress. Mater Manuf Process 32:145–150
25. Johnson GR, Cook WH (1983) A constitutive model and data for metals subjected to large strains, high strain rates and high temperatures. In Proceedings of the 7th International Symposium on Ballistics, The Hague, The Netherlands, pp 541–547
26. Stenberg N, Proudian J (2013) Numerical modelling of turning to find residual stresses. Procedia CIRP 8:258–264
27. Iscar Ltd (2016) Ball nose solid carbide end mills. http://www.iscar.com/eCatalog/Grade.aspx?grade=IC08&item. Accessed 04 April 2016
28. Gonzalo O, Jauregi H, Uriarte G, Lopez de Lacalle LN (2009) Prediction of specific force coefficients from a FEM cutting model. Int J Adv Manuf Technol 43:348–356
29. Stabler GV (1951) Fundamental geometry of cutting tools. Proc Inst Mech Eng 165:14–26
30. Ozturk E, Budak E (2007) Modeling of 5-axis milling processes. Mach Sci Technol 11:287–311